Proceedings of the Twentieth (2010) International Offshore and Polar Engineering Conference
Beijing, China, June 20–25, 2010

ISBN 978-1-880653-77-7 (Set); ISSN 1098-6189 (Set); www.isope.org

Modeling of Wave Breaking and Wave-Structure Interactions by Coupling of Fully Nonlinear Potential Flow and Lattice-Boltzmann Models

Christian F. Janssen[1], *Stéphan T. Grilli*[2] *and Manfred Krafczyk*[1]
1. Technische Universitaet Braunschweig, Institute for Computational Modeling in Civil Engineering, Germany
2. University of Rhode Island, Department of Ocean Engineering, Narragansett, RI, USA

ABSTRACT

In this work, we report on the development and initial validation of a new hybrid numerical model for strongly nonlinear free surface flows, including wave breaking and wave-structure interactions. Specifically, a two-dimensional numerical wave tank (NWT) based on Fully Nonlinear Potential Flow (FNPF) theory, and a higher-order Boundary Element Method (BEM), is used to simulate fully nonlinear wave generation and far-field propagation over a possibly complex, but generally sloping, bottom bathymetry. A particle-based Lattice Boltzmann (LB) model is coupled with (or nested within) the FNPF-NWT, in the region where breaking would normally occur (e.g., upper part of a slope) and interrupt FNPF simulations. The coupled model is able to capture breaking and post-breaking (or wave-interaction) phenomena that involve more complex physics than represented by FNPF theory. Turbulence, in particular, is represented in the LB model by a Large Eddy Simulation (LES) scheme, based on a Smagorinsky model. In applications, we first validate the model for a one-way weakly coupled scheme, in which the LB model is initialized in the near-field, and then possibly driven on its boundary, by the wave-induced far-field velocity and pressure and their derivatives, computed within the NWT. In the paper, we formulate a fully (or strongly) coupled approach, in which the flow is first decomposed into irrotational and viscous perturbation parts. The latter lead to new terms that, by analogy with Navier-Stokes (NS) equations, are expressed as volume forces, that drive LB simulations of the perturbation fields. Applications of this strong coupling approach will be presented at the conference.

KEY WORDS: Fully nonlinear potential flows, Boundary Element Method, Numerical Wave Tank, Lattice-Boltzmann model, LES turbulence model, VOF algorithm, coastal wave breaking

INTRODUCTION

In past work, Grilli et al. performed numerical simulations in two- (2D; (Grilli and Subramanya, 1996)) and three-dimensional (3D; (Grilli et al., 2001)) models based on Fully Nonlinear Potential Flow (FNPF) theory. These models were used to simulate strongly nonlinear wave generation, propagation and shoaling, up to wave overturning, as well as wave structure interactions (i.e., induced motion and forces), and dissipation through breaking or absorption in a numerical beach. These processes take place in the field as well as in laboratory tanks, which has led such models to be referred to as Numerical Wave Tanks (NWTs). The main limitation of FNPF models is that waves cannot be calculated beyond overturning and impact of a breaker jet on the free surface. To do so, models with more complete physics are required. In past work, Grilli et al. coupled their FNPF-NWTs to Navier-Stokes (NS) models (with Volume of Fluid (VOF) interface representation) solving fully turbulent flows (e.g., (Guignard et al., 1999); (Biausser et al., 2004)), thanks to various turbulence models (e.g., LES; (Harris and Grilli, 2010)). In a first type of approach, separate inviscid and viscous domains were used and coupling was achieved through boundary conditions. In a second type of approach, a perturbation method, separating flows into inviscid plus viscous perturbation parts, was used and the solution was carried out in overlapping FNPF and NS domains. In the latter, only the perturbation flows were solved for, which led to very natural homogeneous far-field radiation conditions for these. Here, using the particle-based Lattice Boltzman (LB) method to solve for viscous-turbulent flows, we study both coupling approaches mentioned above (i.e., separate or overlapping domains), between a 2D-FNPF-NWT and a 3D-LB model (LBM), essentially solving similar physics as NS-VOF models, but with specific solver advantages concerning data locality and parallel computing. However, coupling between a continuum mechanics-based model such as the FNPF-NWT and the kinetic LBM is less straightforward than the earlier FNPF-NS coupling. In particular, this requires developing new volumetric forcing terms for the LBM, representing wave-induced momentum input. After a brief presentation of the two underlying numerical methods (FNPF, LBM) we develop equations for achieving the NWT-LBM coupling. Finally, to validate our initial implementation, we present an application to the classical solitary wave shoaling and a breaking over a plane slope.

NUMERICAL WAVE TANK

The 2D-FNPF-NWT used in this work is based on (Grilli and Subramanya, 1996) and (Grilli and Horrillo, 1997)'s implementation. Laplace's equation is solved using a Boundary Element Method (BEM), and 2nd-order Taylor series expansions are used, in an Eulerian-Lagrangian formulation, for the time updating of both the free surface potential and all moving boundary geometries (i.e., free surface, absorbing wavemaker). This requires solving two elliptic problems at each time step, one for the potential and one for its time derivative. Higher-order elements and very accurate numerical integration methods are used in the BEM, which make it possible to achieve extremely high accuracy of the solution and thus to perform long term simulations in the NWT without the need for smoothing or filtering of the solution. In case of long term simulations (e.g., for periodic or irregular waves), an absorbing beach, combining an "absorbing pressure" on the free surface and a lateral absorbing piston wavemaker yields negligible reflection in NWT experiments. Various ways of generating waves are available in the NWT, including flap and piston wavemakers, exact nonlinear waves (both periodic and solitary), and internal sources. Wavemakers can also be used to generate nonlinear random waves based on standard energy spectra. A feedback control loop allows to iteratively modify the wavemaker stroke spectrum to better approach the targeted spectrum.

NWT basics

In accordance with FNPF theory, we introduce a velocity potential $\Phi(x,y,z,t)$, which represents inviscid and irrotational flows in such a way that the velocity is defined as the gradient of the potential $u_i^I = \nabla_i \Phi$. Hence, continuity equation becomes Laplace's equation for the potential

$$\nabla_j \left(u_i^I\right) = \nabla_j (\nabla_i \Phi) = \nabla^2 \Phi = 0. \tag{1}$$

Using Greens 2nd identity, Eq. (1) is transformed into a boundary integral equation (BIE)

$$\alpha(\boldsymbol{x}_l)\Phi(\boldsymbol{x}_l) = \oint_\Gamma \left(G(\boldsymbol{x},\boldsymbol{x}_l) \frac{\partial \Phi(\boldsymbol{x})}{\partial n} - \Phi(\boldsymbol{x}) \frac{\partial G(\boldsymbol{x},\boldsymbol{x}_l)}{\partial n} \right) d\Gamma. \tag{2}$$

with the Green's function

$$G(\boldsymbol{x},\boldsymbol{x}_l) = \frac{-1}{2\pi} \ln r \quad \text{and} \quad \frac{\partial G(\boldsymbol{x},\boldsymbol{x}_l)}{\partial n} = -\frac{1}{2\pi} \frac{\boldsymbol{r}\cdot\boldsymbol{n}}{r^2} \tag{3}$$

with $\boldsymbol{r} = \boldsymbol{x} - \boldsymbol{x}_l$ and $r = |\boldsymbol{r}|$ the distance from point $\boldsymbol{x} = (x,y,z)$ to a point of reference $\boldsymbol{x}_l = (x_l, y_l, z_l)$, both on the boundary, the outward normal vector $\boldsymbol{n}$, and a geometrical parameter $\alpha(\boldsymbol{x}_l) = \theta_l/(2\pi)$, function of the outer angle θ_l of the boundary at position x_l.

Boundary conditions At the stationary parts of the boundary, a no-flow condition is prescribed by specifying zero velocity in the normal direction to the boundary,

$$\frac{\partial \Phi}{\partial n} = 0. \tag{4}$$

For wave generation using a wavemaker, the time-dependent position $\boldsymbol{x}_w$ and velocity $\boldsymbol{u}_w$ of the wavemaker are prescribed via

$$\frac{\partial \Phi}{\partial n} = \boldsymbol{u}_w \cdot \boldsymbol{n} \quad \text{and} \quad \boldsymbol{x} = \boldsymbol{x}_w \tag{5}$$

At the free surface boundary, the non-linear kinematic and dynamic boundary conditions are in Eulerian-Lagrangian form specified as

$$\frac{D\boldsymbol{R}}{Dt} = \boldsymbol{u} = \nabla\Phi \quad \text{and} \quad \frac{D\Phi}{Dt} = -gz + \frac{1}{2}\nabla\Phi\cdot\nabla\Phi - \frac{p_a}{\rho} \tag{6}$$

with free surface position $\boldsymbol{R}$, gravitational acceleration g, atmospheric pressure p_a, fluid density ρ and material derivative D/Dt.

Inner velocities The solution for the velocity potential and its derivatives along the boundary is obtained in the BEM. The values for velocities at any arbitrary point inside the domain u_i^I can be explictly obtained, in a postprocessing step, as a function of the boundary solution for Φ as

$$u_i^I(\boldsymbol{x}) = \oint_\Gamma \left(\nabla G(\boldsymbol{x},\boldsymbol{x}_l) \frac{\partial \Phi(\boldsymbol{x})}{\partial n} - \Phi(\boldsymbol{x}) \nabla \frac{\partial G(\boldsymbol{x},\boldsymbol{x}_l)}{\partial n} \right) d\Gamma. \tag{7}$$

For the calculation of the velocity gradient $\nabla_i u_i^I(\boldsymbol{x})$, the ∇ operator is applied once more to Eq. (7).

THE LATTICE BOLTZMANN METHOD

The LB method has become an increasingly efficient approach for solving a variety of difficult fluid dynamics problems, also in the field of multiphysics. By contrast with classical CFD solvers, which are dealing with the macroscopic Navier-Stokes equations on a continuum basis, the LBM tackles CFD problems on a mesoscopic scale and represents the fluid as a field of particle distribution functions $f(t,\boldsymbol{x},\boldsymbol{\xi})$. Macroscopic hydrodynamic quantities can be obtained from low order moments of these distribution functions. The efficiency and accuracy of the LBM method has been demonstrated in many publications. (Geller et al., 2006) for instance present a study of transient laminar flows. In addition, the method can be efficiently parallelized to benefit from massively parallel hardware (Freudiger et al., 2008). Recently, GPU implementations of a LB method have achieved remarkable performance on graphics processing units (GPUs; see (Tölke, 2008; Tölke and Krafczyk, 2008b) and (Janssen and Krafczyk, 2010)).

LBM basics

The primary variable of microscopic approaches is the particle distribution function $f(t,\boldsymbol{x},\boldsymbol{\xi})$, which specifies the normalized probability to encounter a particle at position $\boldsymbol{x}$ at time t with velocity $\boldsymbol{\xi}$. The evolution of these distribution functions f is described by the Boltzmann equation (Ludwig Boltzmann, 1872):

$$\frac{Df}{Dt} = \frac{\partial f(t,\boldsymbol{x},\boldsymbol{\xi})}{\partial t} + \boldsymbol{\xi}\cdot\frac{\partial f(t,\boldsymbol{x},\boldsymbol{\xi})}{\partial \boldsymbol{x}} = \Omega \tag{8}$$

The left-hand side of this equation is an advection-type expression, while the *collision operator* Ω describes the interactions of particles on the microscopic scale. In order to obtain a model with reduced computational costs, the Boltzmann equation is discretized in the velocity space ξ. In this work, the D3Q19 model (Quian et al., 1992) is used, which introduces the following 19 discretized microscopic particle velocities $\boldsymbol{e}_i = \{0,0,0\},\{\pm c,0,0\},\{0,\pm c,0\},\{0,0,\pm c\},\{\pm c,\pm c,0\},\{\pm c,0,\pm c\},\{0,\pm c,\pm c\}, i = 0,\ldots,18$ where a constant velocity c determines the speed of sound $c_s = c/\sqrt{3}$. The resulting set of discrete Boltzmann equations

$$\frac{Df_i}{Dt} = \frac{\partial f_i(t,\boldsymbol{x})}{\partial t} + \boldsymbol{\xi}_i\cdot\frac{\partial f_i(t,\boldsymbol{x})}{\partial \boldsymbol{x}} = \Omega_i \tag{9}$$

has to be discretized in space and time. This is done using a standard finite difference discretization, in space and time, on a grid with $c = \Delta x/\Delta t$ (grid spacing Δx, time step Δt), which leads to the *lattice* Boltzmann equation,

$$f_i(t+\Delta t,\boldsymbol{x}+\boldsymbol{e}_i\Delta t) - f_i(t,\boldsymbol{x}) = \Omega_i \tag{10}$$

Finally, Eq. (10) may be split up into a non-linear *collision* step, which drives the particle distribution functions to equilibrium locally, and a non-local linear *propagation* step, where the post-collision particle distribution functions are advected to the neighbor nodes as

$$\bar{f}_i(t,\boldsymbol{x}) = f_i(t,\boldsymbol{x}) + \Omega_i \qquad \text{and} \qquad f_i(t+\Delta t,\boldsymbol{x}+\boldsymbol{e}_i\Delta t) = \bar{f}_i(t,\boldsymbol{x}) \tag{11}$$

It has been well-established that solutions of the lattice Boltzmann equation (Eq. (10)) satisfy the incompressible Navier-Stokes equations up to errors of $\mathcal{O}(\Delta x^2)$ and $\mathcal{O}(\mathrm{Ma}^2)$ (Frisch et al., 1987; Junk et al., 2005). The well-known macroscopic values for the hydrodynamic pressure p and macroscopic fluid velocity $\boldsymbol{u}$ are related to the first two hydrodynamic moments of the particle distribution functions as

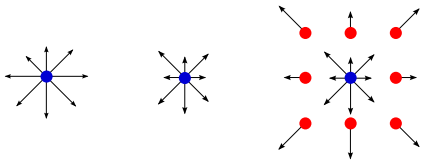

Fig. 1: Collision and propagation

$$p(\boldsymbol{x},t) = c_s^2\rho(\boldsymbol{x},t) = c_s^2\sum_{i=0}^{18} f_i(\boldsymbol{x},t) \qquad \text{and} \qquad \boldsymbol{u}(\boldsymbol{x},t) = \frac{1}{\rho}\sum_{i=0}^{18}\boldsymbol{e}_i f_i(\boldsymbol{x},t) \tag{12}$$

Collision operators

For modelling the interactions between particles, different collision operators Ω_i may be used. In the single relaxation time (SRT) model (Bhatnagar et al., 1954), the particle distribution functions are driven to an equilibrium state with a single relaxation rate. In the more advanced MRT model (d'Humieres et al., 2002), the particle distribution functions are transformed into moment space, where they are relaxed with several different relaxation rates. This increases the stability and at the same time enables the development of more accurate boundary conditions (Ginzburg and D'Humieres, 2003). The moments $\mathbf{m} = \mathsf{M}\cdot\mathbf{f}$ are labeled as

$$\mathbf{m} = \left(\rho, e, \varepsilon, j_x, q_x, j_y, q_y, j_z, q_z, 3p_{xx}, 3\pi_{xx}, p_{ww}, \pi_{ww}, p_{xy}, p_{yz}, p_{xz}, m_x, m_y, m_z\right)^T,$$

and denote the following: mass density $m_0 = \rho$; the part of kinetic energy independent of the density $m_1 = e$; the part of kinetic energy square independent of the density and kinetic energy $m_2 = \varepsilon$; the momentum $m_{3,5,7} = j_{x,y,z}$; $m_{4,6,8} = q_{x,y,z}$ are related to heat flux; $m_{9,11,13,14,15}$ are related to the symmetric traceless viscous stress tensor; $m_{16,17,18}$ are third-order moments; and $m_{10,12}$ are fourth-order moments. The collision operator for MRT is defined as

$$\boldsymbol{\Omega} = \mathsf{M}^{-1}\cdot\mathsf{S}\cdot(\mathsf{M}\cdot\mathbf{f} - \mathbf{m}^{eq}) \tag{13}$$

M denotes the transformation matrix from distribution functions to moments ($\mathbf{m} = \mathsf{M}\cdot\mathbf{f}$ and $\mathbf{f} = \mathsf{M}^{-1}\cdot\mathbf{m}$). The m_i^{eq} are the equilibrium moments. $\mathsf{S} = s_{i,i}$ is the diagonal collision matrix, which contains the relaxation parameters. The parameters

$$s_{9,9} = s_{11,11} = s_{13,13} = s_{14,14} = s_{15,15} = -\frac{\Delta t}{\tau} = s_\omega \tag{14}$$

are related to the kinematic viscosity ν via the relaxation time τ as follows

$$\tau = 3\frac{\nu}{c^2} + \frac{1}{2}\Delta t. \tag{15}$$

The remaining relaxation parameters

$$s_{1,1} = s_a, s_{2,2} = s_b, s_{4,4} = s_{6,6} = s_{8,8} = s_c,$$
$$s_{10,10} = s_{12,12} = s_d \qquad \text{and} \qquad s_{16,16} = s_{17,17} = s_{18,18} = s_e.$$

can be tuned to improve stability (Lallemand and Luo, 2000). While the optimal values for these parameters depend on the specific system under consideration (geometry, initial and boundary conditions), reasonable values are given in (d'Humieres et al., 2002). Here, we use $s_a = s_b = s_c = s_d = s_e = -1.0$.

Smagorinsky LES

In nature, free surface flows usually occur at very high Reynolds numbers, well in the turbulent regime. In order to capture such turbulent flow structures at the sub-grid scale, a Large Eddy Simulation model (LES; (Krafczyk et al., 2003)) is used in combination with the LBM. A spatial filter is applied to the velocity field, which should be fine enough that the larger turbulent structures of the flow do not get filtered out. Hence, only the effect of the smaller sub-grid eddies on the large-scale flow structures is modeled with the LES. This is included in the model through an additional turbulent viscosity ν_T. In the Smagorinsky model ν_T depends on the strain rate tensor, $\nu_\mathrm{T} = (C_S\Delta x)^2\|\mathbf{S}\|$, with Smagorinsky constant C_S and strain rate tensor $S_{\alpha\beta}$, which can be computed locally from the LB moments as

$$S_{\alpha\beta} = \frac{s_{xx}}{2c_s^2\rho}\left(c_s^2\rho\delta_{\alpha\beta} + \rho u_i u_j - P_{\alpha\beta}\right) = \frac{s_{xx}}{2c_s^2\rho}Q_{\alpha\beta} \tag{16}$$

with speed of sound c_s, Dirac delta function δ, density ρ, velocity u, and the second-order moments of the distribution functions P, which can be locally computed from $m_{9,11,13,14,15}$. From Eq. (16) and

$$\tau_\mathrm{total} = \frac{3}{c^2}\nu_\mathrm{total} + \frac{1}{2}\Delta t = \frac{3}{c^2}(\nu_0 + \nu_\mathrm{T}) + \frac{1}{2}\Delta t, \tag{17}$$

a quadratic equation is obtained, which yields

$$\tau_t = \frac{1}{2}\left(\sqrt{\tau_0^2 + 18C_S^2\Delta x^2 Q} - \tau_0\right) \tag{18}$$

and a modified relaxation rate s_{xx} for the second-order moments $m_{9,11,13,14,15}$ of $s_{xx} = \frac{1}{\tau_\mathrm{total}} = \frac{1}{\tau_0+\tau_t}$.

Boundary conditions and volume forces

In the LBM, by nature, boundary conditions have to be directly specified for the distribution functions for the boundary nodes, which is quite different from macroscopic CFD methods.

No-slip boundary and velocity boundary conditions are modeled with a so-called bounce-back scheme, in which the particle distribution function "bounces" off the boundary, as shown in Fig.2a. The incoming missing particle distribution function f_I is reconstructed as

$$f_I^{t+1}(\boldsymbol{x}) = \begin{cases} f_{IA}^{t+1} & = (1-2q)\,f_{iF}^t + 2q\,f_{iA}^t, \quad 0.0 < q < 0.5 \\ f_{IA}^{t+1} & = \frac{2q-1}{2q}\,f_{IA}^t + \frac{1}{2q}\,f_{iA}^t, \quad 0.5 \le q \le 1.0, \end{cases} \tag{19}$$

where i is the inverse direction to I and $\bar{\boldsymbol{u}}$ denotes the prescribed boundary velocity (Bouzidi et al., 2001). The weighting factors w_i for the D3Q19 model are defined as

$$w_0 = \frac{1}{3}, \qquad w_{1..6} = \frac{1}{18} \qquad \text{and} \qquad w_{7..18} = \frac{1}{36} \tag{20}$$

and are given in (He and Luo, 1997).

(a) No-slip (b) Slip

Fig. 2: Wall boundary conditions

At slip boundaries, the bounce forward scheme (Figure 2b) assures that no momentum is modified in tangential direction at the wall. The missing particle distribution function f_I is reconstructed as

$$f_I^{t+1}(\boldsymbol{x}+\boldsymbol{e}_i\boldsymbol{t}) = f_i^t(\boldsymbol{x}) \tag{21}$$

where i is the mirrored direction to I with $\boldsymbol{e}_i\boldsymbol{t} = \boldsymbol{e}_I\boldsymbol{t}$ and $\boldsymbol{e}_i\boldsymbol{n} = -\boldsymbol{e}_I\boldsymbol{n}$ for wall normal vector $\boldsymbol{n}$ and tangential vector $\boldsymbol{t}$.

At the free surface boundary, the anti bounce back rule (Körner et al., 2005) enforces the equality in fluid pressure and surrounding pressure p_B:

$$f_I^{t+1} = -f_i^t + f_I^{eq}(\rho_B, \boldsymbol{u}(t_B,\boldsymbol{x}_B)) + f_i^{eq}(\rho_B, \boldsymbol{u}(t_B,\boldsymbol{x}_B)) \tag{22}$$

where $f_{i,I}^{eq}(\rho_B, \boldsymbol{u}(t_B,\boldsymbol{x}_B))$ are Maxwellian equilibrium distribution functions and ρ_B is related to the surrounding pressure by $\rho_B = p_B c_s^{-2}$.

Gravity and other volume forces $\boldsymbol{F}$ are added directly to the distribution functions f_i in every time step:

$$\Delta f_i = 3\omega_i \rho \boldsymbol{e}_i \cdot \boldsymbol{F}. \tag{23}$$

For transient volume forces, which occur in the coupling to the NWT, a special momentum source term has to be used. (Guo et al., 2002) compare different forcing terms and propose the following formulation, which is also suitable for space- and time-dependent momentum source terms

$$F_i = \left(1 - \frac{1}{2\tau}\right) w_i \left(\frac{\boldsymbol{e}_i - \boldsymbol{v}}{c_s^2} + \frac{\boldsymbol{e}_i \boldsymbol{v}}{c_s^4}\right) \cdot \boldsymbol{F} \tag{24}$$

with weighting factors w_i (Eq. (20)) and density ρ.

Free Surface Model

From a numerical point of view, a free surface represents a moving boundary. Compared to obstacles moving with a predefined velocity, the motion of this boundary is not prescribed, and instead the surface is allowed to move freely. At the same time, the interface has to be kept sharp, although large deformations and even topological changes may occur. In this work, a Volume-Of-Fluid (VOF) approach (Hirt and Nichols, 1981; Youngs, 1982) is used to track the free surface postition, and a fluid fraction variable ε is introduced to describe the *fill level* of a control volume V_{cv}, i.e., the volume fraction being filled with fluid, $\varepsilon = \frac{V_{\text{fluid}}}{V_{\text{cv}}}$. For a unit cell in the LB context (assuming $\Delta x_i = 1.0$), filled with a fluid of density ρ_f and mass m_f, we can state

$$\varepsilon = \frac{m_f/\rho_f}{V_{\text{cv}}} = \frac{m_f}{\rho_f \, \Delta x_1 \, \Delta x_2 \, \Delta x_3} = \frac{m_f}{\rho_f} \tag{25}$$

Thus, a fill level of $\varepsilon = 0.0$ indicates a completely empty cell, while a fill level of $\varepsilon = 1.0$ indicates a completely filled cell.

In standard LB free-surface approaches, the control volumes are directly assigned to the lattice nodes ((Körner et al., 2005), Figure 3a). In contrast to these approaches, we use a staggered grid layout, where every cell (i.e., control volume) is spanned by eight LB nodes. In Figure 3b, the two-dimensional equivalent is shown. A cell is considered fluid if and only if all its vertices are fluid nodes, and a cell is considered gas if and only if all its vertices are gas nodes. All other cells are interface cells. The advantage of this approach is its suitability for a mass-conserving application on non-uniform, block-structured grids. Similar advantages can be seen for combined free-surface and FSI simulations (Janssen and Krafczyk, 2009).

(a) Node-based (b) Cell-based

Fig. 3: Control volumes at a non-uniform block transition

Piecewise linear interface reconstruction In our implementation, a piecewise-linear reconstruction method (PLIC method) is used (Youngs, 1982; Gueyffier et al., 1999). The free surface is represented as a line segment (in 2D) or a plane (in 3D), which can be uniquely described by its unit normal vector $\boldsymbol{n}$ and the distance α to a well-defined point of origin: $\boldsymbol{x} \cdot \boldsymbol{n} = \alpha$ We determine the surface normal vector by a discrete approximation as the gradient of the fluid fraction variable ε:

$$\boldsymbol{n} = -\frac{\nabla \varepsilon}{\|\nabla \varepsilon\|}. \tag{26}$$

This gradient is obtained from the surrounding cell fill levels following (Parker and Youngs, 1992). It can be shown that this approximation is between first- and second-order accurate.

Following this, the only remaining unknown value for the linear surface reconstruction is the distance between the surface plane and a coordinate origin. The expression for the cut volume of a plane and a unit cell with $\Delta x_i = 1.0$ is given by

$$\begin{aligned}\varepsilon(\boldsymbol{n},\alpha) = \frac{1}{2n_1n_2n_3}\Bigg[&\alpha^3 - \sum_{j=1}^{3} H(\alpha - n_j)\left(\alpha - n_j\right)^3 \\ &+ \sum_{j=1}^{3} H(\alpha - \alpha_{max} + n_j)\left(\alpha - \alpha_{max} + n_j\right)^3\Bigg]\end{aligned} \tag{27}$$

with Heaviside function H, $\alpha_{max} = \sum_{j=1}^{3} n_j$, plane parameter α, cell fill level ε, and surface normal vector $\boldsymbol{n}$. Solving analytically for α as an inverse of this expression is not generally possible; therefore, *Brent's method* is used to determine α iteratively (Brent, 1973). The position of the plane can then be uniquely determined.

Discretization of the advection equation The mass exchange between neighboring cells is evaluated from macroscopic velocity and density information on the participating LB nodes. For the weakly compressible LB approach, the sum of fill levels is *not* conserved, so that continuity equation and the principle of conservation of mass must be used to derive the advection algorithm

$$\frac{D\rho}{Dt} = \frac{\partial \rho}{\partial t} + \nabla \cdot (\boldsymbol{v}\rho) = 0 \tag{28}$$

We discretize this equation with a classical finite volume method, by integrating the equation over a control volume and applying the divergence theorem to obtain a boundary integral for the convective term (so called Reynolds Transport Theorem)

$$\int_\Omega \frac{\partial \rho}{\partial t} d\Omega + \int_\Omega \nabla \cdot (\boldsymbol{v}\rho) d\Omega = \frac{\partial}{\partial t}\int_\Omega \rho \, d\Omega + \int_\Gamma (\boldsymbol{v}\rho) \cdot \hat{\boldsymbol{n}} d\Gamma \tag{29}$$

Parameter	Value
Grid	see Table 1
Re	100
Ma	0.017
u_{max}	0.03
BC x	periodic
BC y	periodic
BC z	no-slip

(a) Parameters

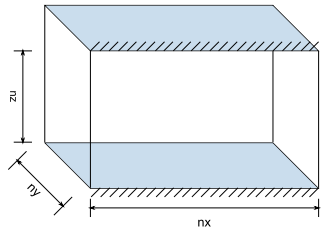

(b) Geometry

Fig. 4: Poiseuille flow between plates

where $\hat{\boldsymbol{n}}$ is the unit outward normal vector on the corresponding face of the control volume. Discretizing in time with an explicit Euler finite difference scheme leads to $m^{t+1} = m^t - \sum_i \Phi_i$ where Φ_i denotes the flux through the ith face of the control volume. The new cell fill level of an interface cell is thus calculated as

$$\varepsilon^{t+1} = \frac{m^{t+1}}{\rho^{t+1}} = \frac{m^t - \sum_i \Phi_i}{\rho^{t+1}} = \frac{\varepsilon^t \rho^t - \sum_i \Phi_i}{\rho^{t+1}} \tag{30}$$

for an unsplit method where all three spatial directions are treated at once.

The fluxes Φ_i are determined using the intersection of the fluid domain and the fraction of the cell volume that is advected, for example, $V_{0,cell} = (v_0 \Delta t)\Delta x_1 \Delta x_2$ in the x_0-direction. The cut volume of a plane and an arbitrary cuboidal control volume with extents Δx_i is given by

$$V(\boldsymbol{n}, \alpha, \Delta x_i) = \frac{1}{2 n_1 n_2 n_3} \left[\alpha^3 - \sum_{j=1}^{3} H(\alpha - \Delta x_j n_j) \left(\alpha - \Delta x_j n_j\right)^3 + \sum_{j=1}^{3} H(\alpha - \tilde{\alpha}_{max} + \Delta x_j n_j) \left(\alpha - \tilde{\alpha}_{max} + \Delta x_j n_j\right)^3 \right] \tag{31}$$

with $\tilde{\alpha}_{max} = \Delta \boldsymbol{x} \cdot \boldsymbol{n} = \sum_{j=1}^{3} \Delta x_j n_j$. This volume V is evaluated for the reconstructed linear surface (normal vector $\boldsymbol{n}$, plane parameter α) and the portion of the cell volume, which is advected to the neighboring cell, $\boldsymbol{v}_i \Delta t$: $\Phi_i = V(\boldsymbol{n}, \alpha, \boldsymbol{v}_i \Delta t)$ for an LB unit cell with $\Delta x_i = 1$.

Algorithmic details The fluxes Φ_i are determined locally for every interface cell, and the mass flux can immediately be balanced. Afterwards, the new fluid nodes must be initialized because they do not contain any distribution functions. The macroscopic values of density and velocity from neighboring old fluid nodes are interpolated:

$$\bar{\rho}(\boldsymbol{x}) = \sum_i w_i \rho(\boldsymbol{x} + \boldsymbol{e}_i) \quad \text{and} \quad \bar{\boldsymbol{v}}(\boldsymbol{x}) = \sum_i w_i \boldsymbol{v}(\boldsymbol{x} + \boldsymbol{e}_i) \tag{32}$$

Based on this information, the particle distribution functions f are initialized with Maxwellian equilibrium distribution functions (Eq. (37)):

$$f_i = f_i^{eq}(\bar{\rho}, \bar{\boldsymbol{v}}) \tag{33}$$

The non-equilibrium part of the distribution functions is then improved with a local, LB-specific, Poisson-type iteration (Mei et al., 2006). In this iteration, a local collision takes place on the new fluid nodes, where the macroscopic velocity is fixed to the above-determined value $\bar{\boldsymbol{v}}$ and the density is allowed to change:

$$\Omega_i = -\frac{\Delta t}{\tau} \left(f_i - f_i^{eq}(\rho, \bar{\boldsymbol{v}})\right) \quad \text{and} \quad \rho = \sum_{i=0}^{18} f_i \tag{34}$$

Eventually, the density converges to the correct nodal density. This minimizes pressure waves induced by incorrect density initialization. Details on the overall algorithm can be found in (Janssen and Krafczyk, 2009).

Validation

Poiseuille flow The performance and accuracy of the LBM fluid solver (with deactivated free surface treatment algorithm) is demonstrated for a Poiseuille flow between plates, using several different grid configurations. In this straightforward problem, the fluid is moving laterally between two plates with infinite length and width. As the grid is refined, the viscosity and the body force are adjusted to match the fixed Reynolds and Mach numbers given in Figure 4a.

The analytical solution for the velocity and pressure profiles is used to check the numerical accuracy of the solver. The flow is driven by a pressure gradient and retarded by viscous drag (mostly in boundary layers) along both plates. Expressing the balance of these forces leads to the following solution for the flow velocity u_x

$$u_x(z) = \frac{z^2 - (0.5 L_z)^2}{2\nu} \frac{dp}{dx} \tag{35}$$

The relative error (in absolute value) between the numerial and analytical solutions for the maximum velocity in the channel is given in Table 1; second-order convergence can clearly be observed with decreasing grid size.

nz	u_{max}	error	rel. error (%)
32	0.0363	6.33E-03	21.121
64	0.0311	1.18E-03	3.946
128	0.0304	4.81E-04	1.605
256	0.0299	3.30E-05	0.110

Table 1: Errors of axial velocity u_{max} as a function of LBM grid size for Re = 100.

Dam breaking After performing the above basic convergence tests, the classic breaking-dam benchmark is used to demonstrate the LB model capability of simulating real-world fluid problems, such as the classical dam break, for which experiments in a scale model were performed (Martin and Moyce, 1952). The main setup is shown in Figure 5. A fluid column in a channel is constrained by a waxed paper diaphragm. The diaphragm is held in position by a thin film of beeswax on a metal strip forming part of the fluid reservoir. An electric current is used to free the waxed paper, initiating the collapse of the water column. Slip boundary conditions are used on the front, bottom, and back walls of the numerical domain. Periodic boundary conditions are applied on the left and right walls. (Martin and Moyce, 1952) determined a maximum dimensionless velocity of $U = 1.71$, which corresponds to Re $\approx 103,483$ and Fr ≈ 2.418.

Param.	Value
a_{exp}	2.25 in
Grid I	100×25
Grid II	200×50
Grid III	300×75
Grid IV	400×100
Re	103483
Fr	2.418
U_{max}	1.71

(a) Parameters

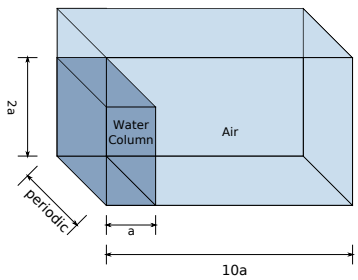

(b) Geometry

Fig. 5: Dam break setup

Fig. 6: Breaking dam, time series

An incompressible MRT scheme, with LES on a uniform grid was used in the LBM for these simulations. Viscosity ν and gravity g are adjusted to match the given dimensionless numbers. Computations are stopped when the surge front reaches the back wall of the domain (container).

Results for four different grid resolutions are compared with the experimental benchmark data from (Martin and Moyce, 1952) in Figure 7a and Figure 7b. Very good agreement can be seen in Figure 7a, for the height of the collapsing water column, even at low resolutions. However, the numerical surge front (Figure 7b) evolves faster than the experimental one. This might be due to the fact that the slight delay in triggering the flow in experiments (using a thin diaphragm that is released by an electric current) is not modeled in our numerical simulations. This effect was also observed by e.g. (Salih and Moulic, 2006).

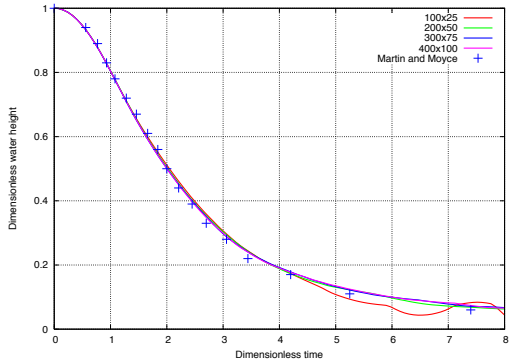

(a) Position of the water column top

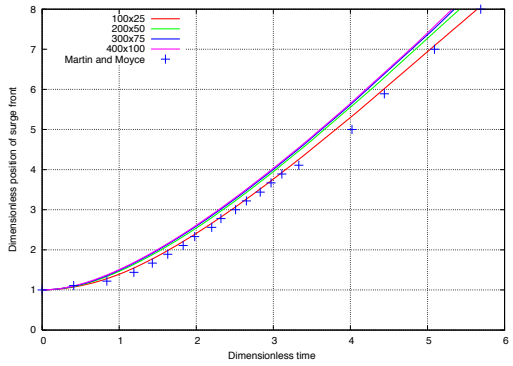

(b) Position of the surge front

Fig. 7: Breaking dam, comparison of numerical and experimental results

NWT-LB COUPLING

For complex fluid simulations, a hybrid model is desirable, combining the advantages of both FNPF and LBM frameworks. Indeed, potential flow theory is no longer applicable near rigid structures, in the surfzone or around steep bottom obstacles, where strongly nonlinear interactions, local wave breaking or significant vortex shedding and viscous dissipation occur. Moreover, the size of the LBM domain is limited, mainly due to computational expenses, and cannot meaningfully be used for the whole domain. Hence, a highly resolved and/or turbulent LBM simulation should only be performed in the vicinity of a structure or a wave breaking region, and not in the peripheral regions of the flow field.

Weak coupling

In a weakly coupled approach the LB domain is initialized with results of the NWT. Only this initial, unidirectional coupling is specified. At the fluid boundary (Figure 8), non-transient boundary conditions for the water height $\bar{h} = h^{NWT}(t=0)$ and a constant inflow velocity $\bar{\boldsymbol{v}} = \boldsymbol{v}^{NWT}(t=0)$ are prescribed.

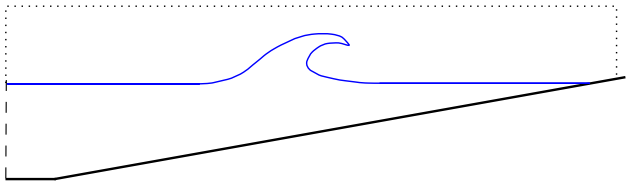

Fig. 8: Initialization of the entire LBM domain with the inviscid, irrotational NWT solution u^I, p^I

In the LBM, based on this information, the particle distribution functions f are initialized with Maxwellian equilibrium distribution functions

$$f_i = f_i^{eq}(\bar{\rho}, \bar{\boldsymbol{v}}) \tag{36}$$

The equilibrium distribution functions tuned for incompressible flows are

$$f_i^{eq} = w_i \left[\rho + \rho_0 \left(3\frac{\boldsymbol{e}_i \cdot \boldsymbol{u}}{c^2} + \frac{9}{2}\frac{(\boldsymbol{e}_i \cdot \boldsymbol{u})^2}{c^4} - \frac{3}{2}\frac{u^2}{c^2} \right) \right] \tag{37}$$

where ρ_0 is the reference density and w_i are weighting factors according to Eq. (20). Alternately, a local Poisson-type iteration might be used to further improve the non-equilibrium parts of the distribution functions, ((Mei et al., 2006), Eq. (34)).

This weakly coupled approach requires to model the total flow in the LBM. Moreover, the size of the LB domain must be large enough to avoid perturbations from the non-transient boundary condition.

Weak coupling with transient boundary conditions In order to reduce the domain size, transient boundary conditions may be used (Figure 8) and time-dependent values for velocity and position of the free surface can be prescribed on the leftward boundary ($\bar{\boldsymbol{v}}(t) = \boldsymbol{v}^{NWT}(t)$).

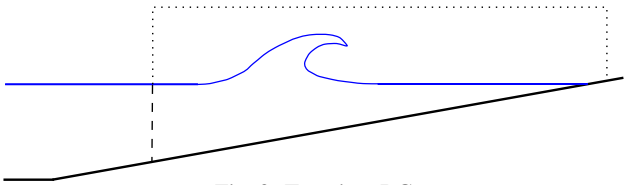

Fig. 9: Transient BC

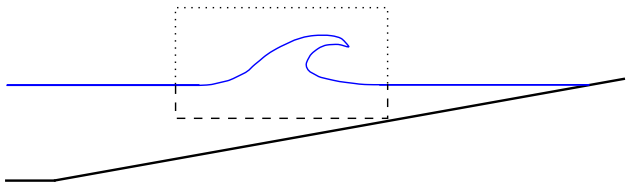

Fig. 10: Transient BCs or perturbation approach

Strong coupling

In the strongly coupled approach, the NWT does not only serve to initialize the LB computations, but also drives computations either via transient boundary conditions, or via volumetric source terms in the momentum equation. In both cases the domain size can be reduced significantly (Figure 10).

For wave-induced flows, the viscous perturbation caused by a structure, bottom geometry, or a beach onto the otherwise nearly inviscid, irrotational flow is expressed explicitly in the model. As indicated before, pressure and velocity field are split up into the irrotational, inviscid part p^I, u^I and the rotational, viscous perturbation p^P, u^P

$$u_i = u_i^I + u_i^P \qquad \text{and} \qquad p = p^I + p^P. \tag{38}$$

with u_i^I obtained from the NWT, while the LBM solves for u_p. The inviscid far-field wave flow is specified into the LBM via volumetric terms, which can be expressed, by analogy, by inserting Eq. (38) into the NS equations

$$\frac{\partial u_i}{\partial t} + u_j \frac{\partial u_i}{\partial x_j} = -\frac{1}{\rho}\frac{\partial p}{\partial x_i} + (\nu + \nu_T)\frac{\partial^2 u_i}{\partial x_j^2} + \frac{\partial \nu_T}{\partial x_j}\left(\frac{\partial u_i}{\partial x_j} + \frac{\partial u_j}{\partial x_i}\right) \tag{39}$$

with velocity u_i, pressure p, viscosity ν and turbulent viscosity ν_T. After transformation, we have,

$$\frac{\partial u_i^P}{\partial t} + u_j^P \frac{\partial u_i^P}{\partial x_j} = -\frac{1}{\rho}\frac{\partial p^P}{\partial x_i} + (\nu + \nu_T)\frac{\partial^2 u_i^P}{\partial x_j^2} + \frac{\partial \nu_T}{\partial x_j}\left(\frac{\partial u_i^P}{\partial x_j} + \frac{\partial u_j^P}{\partial x_i}\right) \underbrace{-u_i^I \frac{\partial u_i^P}{\partial x_j} - u_j^P \frac{\partial u_i^I}{\partial x_j} + \frac{\partial \nu_T}{\partial x_j}\left(\frac{\partial u_i^I}{\partial x_j} + \frac{\partial u_j^I}{\partial x_i}\right)}_{Additional\ terms} \tag{40}$$

where u_i^I, the irrotational velocity field, satisfies Euler equations. One can see that, in addition to viscous and turbulent terms on the right hand side, convection-like interaction terms between u_i^I und u_i^P occur. Besides those additional source terms

$$F_i = -u_i^I \frac{\partial u_i^P}{\partial x_j} - u_j^P \frac{\partial u_i^I}{\partial x_j} + \frac{\partial \nu_T}{\partial x_j}\left(\frac{\partial u_i^I}{\partial x_j} + \frac{\partial u_j^I}{\partial x_i}\right) \tag{41}$$

corresponds to Eq. (39). The velocity u_i^I and the velocity gradient are obtained from the NWT's solution at the current time step, while the perturbating part and its gradients are obtained from values of the previous time step LB solution.

Parametrization

In order to transfer the simulation results from the NWT to the LB model, a parametrization has to be established, to select the LB parameters for grid spacing Δx, Mach number Ma, forcing g_{LB} and viscosity ν. This involves three steps.

First, as the solutions of the LBM satisfies NS equations, up to an order $\mathcal{O}(Ma^2)$, it is indispensable to observe and prescribe the maximum Mach number Ma and hence the maximum velocity $v_{max} = \mathrm{Ma} \cdot c_s = \mathrm{Ma} \cdot \frac{c}{\sqrt{3}}$ in the LB simulation. Second, free surface flows are qualified by their Froude number, i.e., a dimensionless number that compares inertia and gravitational forces, $Fr = v\,(gh)^{-0.5}$ using maximum velocity v, gravity g and water depth h. The Froude numbers of the NWT and the LBM must be identical, so that based on a given LB discretization we can calculate the LB gravitational term $g_{LB} = v_{max}^2 \mathrm{Fr}^{-2} h_{LB}^{-1}$. Third, the Reynolds number of experiments and numerical simulations should be the same. The NWT is based on inviscid potential flow theory, so that a Reynolds number cannot be assigned. Nonetheless we can calculate a corresponding Reynolds number via $Re = \frac{vD}{\nu_{water}}$ and, consequently, find the resulting LB viscosity as $\nu_{LB} = v_{LB} h_{LB} \mathrm{Re}^{-1}$

Finally, we find that NWT results for velocity and pressure should be transferred to the LB simulations by applying the following scaling factors

$$\Delta v = \frac{v_{max,LB}}{v_{max,NWT}} \qquad \text{and} \qquad \Delta x = \frac{h_{LB}}{h_{NWT}} \tag{42}$$

$$\Delta t = \frac{\Delta x}{\Delta v} \qquad \text{and} \qquad \Delta p = \frac{\rho_{LB} g_{LB} h_{LB}}{\rho_{NWT} g_{NWT} h_{NWT}} \tag{43}$$

It turns out that the only free parameters in these equations are the grid resolution (which directly governs Δx) and the Mach number limit ($\mathrm{Ma}_{max} = 0.1$ is considered a reasonable maximum value for an incompressible limit).

RESULTS

Breaking wave

The application of the weakly coupled algorithm is illustrated for the case of a solitary wave that breaks during shoaling. The LB domain measures $600 \times 1 \times 90$ lattice nodes. Maximum Mach number is fixed to $\mathrm{Ma} = 0.04$, the remaining dimensionless parameters are found as: $\mathrm{Re} \approx 630{,}000$ and $\mathrm{Fr} \approx 0.84$, resulting in a body force $g_{LB} = 1.81E-5$ and a viscosity $\nu_{LB} = 1.505E-6$. Initial results of the LB simulations for velocity and pressure fields are shown in Figure 11 for a solitary wave of height $H = 0.5m$ over a 1:15 slope. In Figure 12, a time series of the free surface evolution is given for selected time steps. The general expected flow behaviour is well represented, although the breaker jet is slightly thicker compared to results of purely potential flow simulations (e.g., (Grilli et al., 1997)).

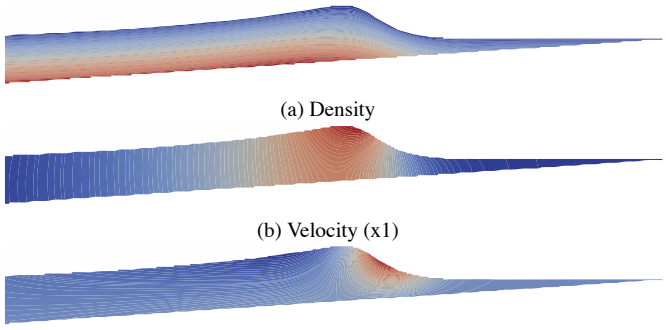

(a) Density

(b) Velocity (x1)

(c) Velocity (x3)

Fig. 11: Initialization of the LBM domain with NWT data

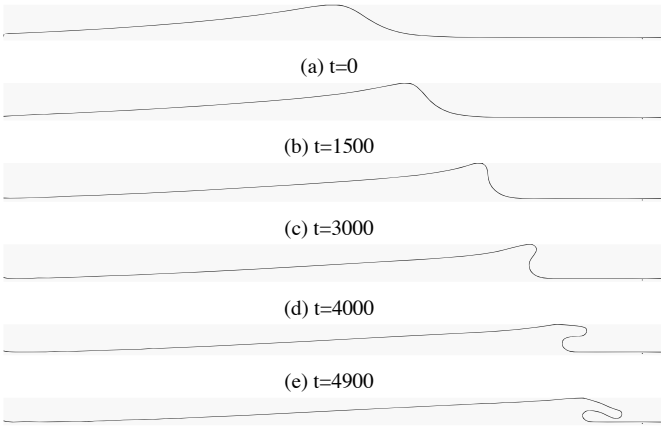

Fig. 12: Snapshots of the simulation

CONCLUSIONS

Although the computations shown in the results section are very preliminary and should thus be further examined, we presented a new hybrid FNPF-LBM approach, which already shows promising results. We believe that our hybrid method will turn out to be a numerical tool, able to accurately and efficiently investigate wave breaking phenomena and wave structure interactions. However, the full advantage of the method will only reveal itself when applications of the strong coupling approach are presented, which is work in progress.

REFERENCES

[Bhatnagar et al., 1954] Bhatnagar, P. L., Gross, E. P., and Krook, M. (1954). A model for collision processes in gases. i. small amplitude processes in charged and neutral one-component systems. *Phys. Rev.*, 94(3):511–525.

[Biausser et al., 2004] Biausser B., S.T.Grilli, Fraunie P. and Marcer, R. (2004). Numerical analysis of the internal kinematics and dynamics of three-dimensional breaking waves on slopes. *International Journal of Offshore and Polar Engineering,* 14(4):247-256.

[Bouzidi et al., 2001] Bouzidi, M., Firdaouss, M., and Lallemand, P. (2001). Momentum transfer of a lattice-boltzmann fluid with boundaries. *Physics of Fluids*, 13:3452–3459.

[Brent, 1973] Brent, R. P. (1973). *Algorithms for Minimization Without Derivatives*. Prentice Hall. Reviewed in: American Scientist 61 (May-June 1973), 374; Mathematical Programming 4 (1973), 349; Computer J. 16 (1973), 314; Math. Comp. 28 (1974), 865-866;.

[d'Humieres et al., 2002] d'Humieres, D., Ginzburg, I., Krafczyk, M., Lallemand, P., and Luo, L.-S. (2002). Multiple Relaxation-Time Lattice Boltzmann models in three-dimensions. *Royal Society of London Philosophical Transactions Series A*, 360:437–451.

[Freudiger et al., 2008] Freudiger, S., Hegewald, J., and Krafczyk, M. (2008). A parallelization concept for a multi-physics lattice boltzmann solver based on hierarchical grids. *Progress in Computational Fluid Dynamics*, 8(1-4):168–178.

[Frisch et al., 1987] Frisch, U., d'Humières, D., Hasslacher, B., Lallemand, P., Pomeau, Y., and Rivet, J.-P. (1987). Lattice Gas Hydrodynamics in Two and Three Dimensions. *J. Complex Syst.*, 1:75–136.

[Geller et al., 2006] Geller, S., Krafczyk, M., Tölke, J., Turek, S., and Hron, J. (2006). Benchmark computations based on Lattice-Boltzmann, Finite Element and Finite volume Methods for laminar Flows. *Comp. and Fluids*, 35:888–897.

[Ginzburg and D'Humieres, 2003] Ginzburg, I. and D'Humieres, D. (2003). Multireflection boundary conditions for lattice Boltzmann models. *Physical Review E*, 68(6):066614.1–066614.30.

[Grilli and Horrillo, 1997] Grilli, S.T. and Horrillo, J. (1997). Numerical Generation and Absorption of Fully Nonlinear Periodic Waves. *Journal of Engineering Mechanics*, 123(10):1060-1069.

[Grilli and Subramanya, 1996] Grilli, S.T. and Subramanya, R. (1996). Numerical Modeling of Wave Breaking Induced by Fixed or Moving Boundaries. *Computational Mechanics*, 17(6):374-391.

[Grilli et al., 2001] Grilli, S., Guyenne, P., and Dias, F. (2001). A fully nonlinear model for three-dimensional overturning waves over arbitrary bottom. *International Journal for Numerical Methods in Fluids*, 35(7):829 – 867.

[Grilli et al., 1997] Grilli, S.T., Svendsen, I.A. and Subramanya, R. (1997). Breaking Criterion and Characteristics for Solitary Waves on Slopes. *Journal of Waterway Port Coastal and Ocean Engineering,* 123(3):102-112.

[Guignard et al., 1999] Guignard, S., Grilli, S.T., Marcer, R. and Rey, V. (1999). Computation of shoaling and breaking waves in nearshore areas by the coupling of BEM and VOF methods. *In Proc. 9th Offshore and Polar Engng. Conf.* (ISOPE99, Brest, France, May 1999), Vol. III, 304-309.

[Gueyffier et al., 1999] Gueyffier, D., Li, J., Nadim, A., Scardovelli, R., and Zaleski, S. (1999). Volume-of-fluid interface tracking with smoothed surface stress methods for three-dimensional flows. *Journal of Computational Physics*, 152(2):423–456.

[Guo et al., 2002] Guo, Z., Zheng, C., and Shi, B. (2002). Discrete lattice effects on the forcing term in the lattice Boltzmann method. *Physical Review E*, 65(4):046308.1 – 046308.6.

[Harris and Grilli, 2010] Harris, J. and Grilli, S.T. (2010). Coupling of NWT and large eddy simulation for wave-induced sediment transport. (this conference).

[He and Luo, 1997] He, X. and Luo, L.-S. (1997). Lattice boltzmann model for the incompressible navier-stokes equation. *Journal of Statistical Physics*, 88:927–944.

[Hirt and Nichols, 1981] Hirt, C. and Nichols, B. (1981). Volume of fluid method for dynamics of free boundaries. *Journal of Computational Physics*, 39:201–221.

[Janssen and Krafczyk, 2009] Janssen, C. and Krafczyk, M. (2009). A lattice Boltzmann approach for free-surface-flow simulations on non-uniform block-structured grids. *Computers and Mathematics with Applications*.

[Janssen and Krafczyk, 2010] Janssen, C. and Krafczyk, M. (2010). Free surface flow simulations on GPUs using LBM. *submitted to: CAMWA*.

[Junk et al., 2005] Junk, M., Klar, A., and Luo, L.-S. (2005). Asymptotic analysis of the lattice boltzmann equation. *Journal of Computational Physics*, 210(2):676–704.

[Körner et al., 2005] Körner, C., Thies, M., Hofmann, T., Thürey, N., and Rüde, U. (2005). Lattice boltzmann model for free surface flow for modeling foaming. *Journal of Statistical Physics*, 121(1-2):179–196(18).

[Krafczyk et al., 2003] Krafczyk, M., Tölke, J., and Luo, L.-S. (2003). Large-eddy simulations with a multiple-relaxation-time LBE model. *Int. J. Mod. Phys. B*, 17:33–39.

[Lallemand and Luo, 2000] Lallemand, P. and Luo, L.-S. (2000). Theory of the lattice boltzmann method: Dispersion, dissipation, isotropy, galilean invariance, and stability. *Physical Review*, E 61:6546–6562.

[Martin and Moyce, 1952] Martin, J. and Moyce, W. (1952). An experimental study of the collapse of liquid columns on a rigid horizontal plane. Technical report.

[Mei et al., 2006] Mei, R., Luo, L.-S., Lallemand, P., and d'Humieres, D. (2006). Consistent initial conditions for lattice boltzmann simulations. *Computers & Fluids*, 35(8-9):855 – 862.

[Parker and Youngs, 1992] Parker, B. and Youngs, D. (1992). Two and three dimensional eulerian simulation of fluid flow with material interfaces. Technical report, UK Atomic Weapons Establishment.

[Quian et al., 1992] Quian, Y. H., d'Humieres, D., and Lallemand, P. (1992). Lattice BGK models for Navier Stokes equations. *Europhysics Letters*, 17:479–484.

[Salih and Moulic, 2006] Salih, A. and Moulic, S. G. (2006). A level set formulation for the numerical simulation of impact of surge fronts. *SADHANA - Academy Proceedings in Engineering Sciences*, 31:697–707.

[Tölke, 2008] Tölke, J.(2008). Implementation of a lattice boltzmann kernel using the compute unified device architecture developed by nvidia. *Computing and Visualization in Science*, 1:29 – 39.

[Tölke and Krafczyk, 2008b] Tölke, J. and Krafczyk, M. (2008b). Teraflop computing on a desktop pc with gpus for 3d cfd. *International Jounrla of Computational Fluid Dynamics*, 22:443 – 456.

[Youngs, 1982] Youngs, D. (1982). Time-dependent multimaterial flow with large fluid distortion. In Morton, K. and Baines, M., editors, *Numerical Methods for Fluid Dynamics*, pages 273–285. Academic Press.